PHOTONIC SENSORS / Vol. 11, No. 4, 2021: 402–410

Distributed Fiber Birefringence Measurement Using Pulse-Compression Φ-OTDR

Yongxiang CHEN, Yun FU, Ji XIONG, and Zinan WANG*

Key Lab of Optical Fiber Sensing & Communications, University of Electronic Science &Technology of China, Chengdu 611731, China

*Corresponding author: Zinan WANG E-mail: znwang@uestc.edu.cn

Abstract: In this paper, a novel birefringence measurement method through the Rayleigh backscattered lightwave within single-mode fiber is proposed, using a single chirped-pulse with arbitrary state of polarization. Numerical analysis is carried out in detail, then pulse-compression phase-sensitive optical time domain reflectometry (PC-Φ-OTDR) with polarization-diverse coherent detection is employed to verify this method. A 2 km spun single-mode fiber is tested with 8.6 cm spatial resolution, and the average birefringence of the fiber under test is measured as 0.234 rad/m, which is consistent with previous literatures about single-mode fiber. Moreover, the relationship between the measured birefringence and the spatial resolution is also studied for the first time, and the results show that spatial resolution is crucial for fiber birefringence measurement.

Keywords: Birefringence; Rayleigh scattering; pulse-compression; phase-sensitive optical time-domain reflectometry; coherent detection; polarization-diverse receiver

Citation: Yongxiang CHEN, Yun FU, Ji XIONG, and Zinan WANG, "Distributed Fiber Birefringence Measurement Using Pulse-Compression Φ-OTDR," *Photonic Sensors*, 2021, 11(4): 402–410.

1. Introduction

As an internal propagation characteristic of the fibers, birefringence is related to the perturbation of anisotropy due to waveguide imperfections [1] and environmental changes, such as twisting, bending, and temperature fluctuating [2]. As a result, it plays a significant role in telecommunications [3] and some fiber sensors [4, 5]. Therefore, measuring the distribution of birefringence becomes necessary in order to optimize the quality of manufacture process and evaluate the change of environment, etc.

There are three common methods for measuring fiber birefringence, which respectively are based on Sagnac interferometer, Faraday effect, and scattering inside optical fiber.

The Sagnac interferometer can be used to measure the birefringence of fibers [6–8], since different loop birefringence will cause different intensity transfer functions. However, since its periodic transmission function is extremely broad, this system cannot measure a short section of a low-birefringence fiber. For the purpose of improving this system, Kim *et al.* [8] proposed a two-segment Lyot-Sagnac fiber interferometer, but this system was limited by the refraction index difference-length product of the fiber in the 10^{-3} m to 10^{-6} m range. As a result, this interferometer needs an extremely long fiber to measure its low birefringence (low refraction index difference) and it does not allow distributed measurement.

The measurement method for ultralow

Received: 01 May 2020 / Revised: 31 July 2020

DOI: 10.1007/s13320-020-0604-3
Article type: Regular

birefringence based on the Faraday magneto-optic effect was proposed in 1990s [9]. The intrinsic birefringence of fiber will change the Faraday rotation angle, so analyzing the output plane of polarization provides a measurement of the birefringence. The linear birefringence of 10^{-8} could be measured with 5% measurement accuracy in meter-long optical fibers [10]. However, such methods have strict requirements for the polarization alignment—the angles between the polarization of the input linearly polarized light and the principal axis of the Wollaston prism should be precisely adjusted to 45°.

The scattering-based birefringence measurement scheme includes two typical types, which are Brillouin-scattering (BS) based [11, 12] birefringence measurement systems and Rayleigh-scattering (RS) based [13–17] birefringence measurement systems. As for the BS based systems, Lu *et al.* [12] proposed a system with beat period detection of homodyne Brillouin optical time-domain reflectometry (BOTDR), but this system's signal-to-noise ratio (SNR) highly depends on the input pulses' state of polarization (SOP) and it takes 80 seconds to complete once measurement. As for the RS based systems, Soto *et al.* [15] used the polarization correlation in phase-sensitive optical time-domain reflectometry to distributedly achieve phase birefringence measurement. Through two beams of orthogonally-polarized light, metric spatial resolution and 10^{-7} minimum detectable index difference are implemented. However, this kind of systems strictly needs two input lightwaves along the principal axes of the fiber and multiple input pulses with different frequencies. After that, Liu *et al.* [16] adopted the quaternion approach with direct detection to avoid multiple pulses, but the detection module involves free space optical components, which is too complicated. For example, when measuring the state of polarization, if detection module involves free space optical components, these components need to be adjusted during the measurement to ensure that no additional errors are introduced, such as the polarization alignment of the optical components.

In this paper, at first a novel measurement principle for the birefringence along the single-mode fiber (SMF) is described in detail. Then, the experiment based on the pulse-compression phase-sensitive optical time domain reflectometry (PC-Φ-OTDR) [18] with polarization-diverse coherent detection is implemented, proving the validity and the flexibility of this method. Compared with the traditional Φ-OTDR, the input signal for PC-Φ-OTDR used is changed from a single pulse to a chirped pulse. Pulse compression is used when the signal is demodulated to obtain the equivalent single pulse response of the system, and finally the birefringence of the fiber is measured. Due to the use of chirped pulses, the entire experimental system can bring about higher spatial resolution without sacrificing the signal-to-noise ratio. The experimental results show that the average birefringence of the 2 km spun SMF under test is 0.234 rad/m, which is consistent with the reported results in previous literatures. Since PC-Φ-OTDR could provide unprecedented spatial resolution (with chirped pulse) for Rayleigh-scattering-based birefringence measurement, the dependence of birefringence on spatial resolution is also investigated for the first time, and the experimental results match well with the numerical results.

Compared with previous methods [6–17], the proposed method only needs a single pulse with arbitrary SOP to retrieve the distribution of birefringence. Besides, the detection module only uses a 90° optical hybrid and two balance photo-detectors, which does not involve any polarization alignment. In addition, this is the first time that the quantitative relationship between spatial resolution and measured birefringence has been revealed.

2. Measurement principles

The proposed approach is essentially based on the SOP of the Rayleigh backscattered (RBS)

lightwaves. The theoretical background is elaborated in this section.

2.1 Birefringence in fibers

For the fiber under test, the scattering process will cancel out the effect of circular birefringence, so the circular birefringence is ignored in the following analysis. Ignoring the fiber attenuation, there are two ways to represent the transmission process with Stokes vectors [19, 20], as shown in (1)

$$\begin{cases} \dfrac{\mathrm{d}\mathbf{S}(z)}{\mathrm{d}z} = \mathbf{S}(z)\times\mathbf{S}(z) \\ \mathbf{S}(z)=\mathbf{M}(z)\mathbf{S}_0 \end{cases} \tag{1}$$

where $\mathbf{S}_0$ and $\mathbf{S}(z)$ are the Stokes vectors of input light and output light; $\mathbf{M}(z)$ is the Mueller matrix; $\boldsymbol{\beta}(z)=\begin{pmatrix}\beta_1 & \beta_2 & 0\end{pmatrix}^{\mathrm{T}}$ is the birefringence of the fiber, and the local linear birefringence equals to $\beta_l=\sqrt{\beta_1^2+\beta_2^2}$.

By further integrating the two formulas in (1), the relationship between the fiber Mueller matrix $\mathbf{M}(z)$ and the birefringence vector $\boldsymbol{\beta}(z)$ can be obtained, as shown in (2)

$$\frac{\mathrm{d}[\mathbf{M}(z)]}{\mathrm{d}z}\mathbf{M}^{-1}(z)\mathbf{S}(z)=\boldsymbol{\beta}(z)\times\mathbf{S}(z). \tag{2}$$

Similar to (2), the relationship between RBS lightwave $\mathbf{S}_B(z)$ and birefringence $\boldsymbol{\beta}(z)$ could be deduced as [18]

$$\frac{\mathrm{d}\mathbf{S}_B(z)}{\mathrm{d}z}=2\mathbf{M}_s\mathbf{M}^{\mathrm{T}}\begin{pmatrix}\beta_1\\ \beta_2\\ 0\end{pmatrix}\times\mathbf{S}_B(z) \tag{3}$$

where $\mathbf{M}_s$ is the diagonal matrix of $\mathrm{diag}(1,\ 1,\ -1)$, and $\mathbf{M}$ is the Muller matrix $\mathbf{M}(z)$. Reference [19] pointed out $\mathbf{M}$ for a segment fiber:

$$\mathbf{M}=\begin{pmatrix} \cos^2 2\theta+\sin^2 2\theta\cos\gamma & \sin 2\theta\cos 2\theta(1-\cos\gamma) & \sin\gamma\sin 2\theta \\ \sin 2\theta\cos 2\theta(1-\cos\gamma) & \sin^2 2\theta+\cos^2 2\theta\cos\gamma & -\sin\gamma\cos 2\theta \\ -\sin\gamma\sin 2\theta & \sin\gamma\cos 2\theta & \cos\gamma \end{pmatrix} \tag{4}$$

where γ is the fiber's linear birefringence, and θ is the angle between the fast axis and the *x*-axis of the reference frame. Thus, the birefringence of the fiber could be written as $\boldsymbol{\beta}=\gamma\begin{pmatrix}\cos 2\theta & \sin 2\theta & 0\end{pmatrix}^{\mathrm{T}}$. Therefore, backward birefringence $\boldsymbol{\beta}_B$ equals

$$\begin{aligned} \boldsymbol{\beta}_B &= 2\mathbf{M}_S\mathbf{M}^{\mathrm{T}}\boldsymbol{\beta} \\ &= 2\gamma\begin{pmatrix} \cos^2 2\theta+\sin^2 2\theta\cos\gamma & \sin 2\theta\cos 2\theta(1-\cos\gamma) & -\sin\gamma\sin 2\theta \\ \sin 2\theta\cos 2\theta(1-\cos\gamma) & \sin^2 2\theta+\cos^2 2\theta\cos\gamma & \sin\gamma\cos 2\theta \\ \sin\gamma\sin 2\theta & -\sin\gamma\cos 2\theta & -\cos\gamma \end{pmatrix}\begin{pmatrix}\cos 2\theta\\ \sin 2\theta\\ 0\end{pmatrix} \\ &= 2\gamma\begin{pmatrix} \left(\cos^2 2\theta\cos 2\theta+\sin^2 2\theta\cos 2\theta\right)+\left(\sin^2 2\theta\cos 2\theta\cos\gamma-\sin^2 2\theta\cos 2\theta\cos\gamma\right) \\ \left(\sin 2\theta\cos^2 2\theta+\sin^2 2\theta\sin 2\theta\right)+\left(\cos^2 2\theta\cos\gamma\sin 2\theta-\sin 2\theta\cos^2 2\theta\cos\gamma\right) \\ 0 \end{pmatrix} \\ &= 2\boldsymbol{\beta}. \end{aligned} \tag{5}$$

As a result, (3) could be written as

$$\frac{\mathrm{d}\mathbf{S}_B(z)}{\mathrm{d}z}=2\boldsymbol{\beta}(z)\times\mathbf{S}_B(z). \tag{6}$$

Equation (6) means that $\mathbf{S}_B$ rotates around $\boldsymbol{\beta}_B(z)$ on the Poincaré sphere, and the rotating angle induced by $\boldsymbol{\beta}_B(z)$ equals twice of the angle induced by $\boldsymbol{\beta}(z)$.

2.2 Measuring approach for the birefringence distribution

The long standard single-mode fiber can be modeled as a series of short fiber sections, each of which has uniform polarization characteristics. The brief diagram of the model is similar with the model in [19], the polarization mode dispersion (PMD) is not considered, and the circular birefringence is

ignored.

The SOPs of RBS lightwave are represented by $\mathbf{S}_{B,i}$ $(i/3=1, 2, 3, \cdots)$ and the round-trip birefringence vector is $\boldsymbol{\beta}_{B,i}$. Δz is the distance between two consecutive sampling points. In the low birefringence SMF, when the distance between two consecutive sampling points Δz is much smaller than the beat length, it could be assumed that the linear birefringence of any three adjacent sampling points is equal in magnitude.

Equation (6) points out that the arbitrary three adjacent Stokes vectors of the RBS lightwave, namely, $\mathbf{S}_{B,i}$, $\mathbf{S}_{B,i+1}$, and $\mathbf{S}_{B,i+2}$, locate on the surface of the Poincaré sphere with in a circle. Figure 1 shows a more intuitive understanding of (6). $\mathbf{S}_{B,i+1}$ is formed by rotating $\mathbf{S}_{B,i}$ around $\boldsymbol{\beta}_{B,i}$ with the angle of θ_1, and $\mathbf{S}_{B,i+2}$ is formed by rotating $\mathbf{S}_{B,i+1}$ around $\boldsymbol{\beta}_{B,i+1}$ with the angle of θ_2 ($\theta_2=\theta_1$). It is worth noting that the rotary axis $\mathbf{n}$ of the adjacent three backscattered lights on the Poincaré sphere does not directly reflect the vector information of the local birefringence.

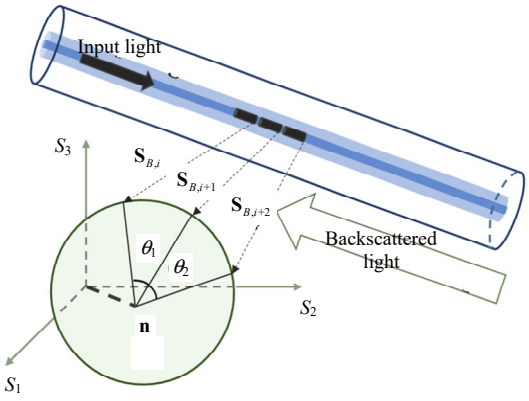

Fig. 1 Evolution of backscattered Stokes vectors within arbitrary three adjacent segments.

The rotation angle in Fig. 1 is $\theta_1=2\left|\boldsymbol{\beta}_{B,i}\right|\Delta z$, which depicts that if the value of θ_1 is obtained, birefringence distribution can be retrieved. According to the SOPs of the backscattered lights, the modules of the birefringence can be extracted by using the geometric relationship shown in (7)

$$\theta_1=2\left|\boldsymbol{\beta}_{B,i}\right|\Delta z=\arccos\left(\frac{\left(\mathbf{S}_{B,i+2}-\mathbf{S}_{B,i+1}\right)\cdot\left(\mathbf{S}_{B,i+1}-\mathbf{S}_{B,i}\right)}{\left|\mathbf{S}_{B,i+2}-\mathbf{S}_{B,i+1}\right|\left|\mathbf{S}_{B,i+1}-\mathbf{S}_{B,i}\right|}\right). \tag{7}$$

2.3 SOPs detected using 90° optical hybrid

When the Rayleigh backscattered signal and the local oscillator are mixed with the 90° optical hybrid, two detectors can be used to obtain the intensities of two orthogonal polarized lights [21, 22]. Then, after Hilbert transforming, the intensities and the phases of two orthogonal polarized lights (with $\mathbf{E}_x$ and $\mathbf{E}_y$ represented, respectively) are obtained [23]. By using the definition of Stokes vectors [24], which is shown in (8), the SOPs of the backscattered lights could be obtained.

$$\begin{aligned} S_0&=\left\langle\left|\mathbf{E}_x\right|^2+\left|\mathbf{E}_y\right|^2\right\rangle,\ S_1=\left\langle\left|\mathbf{E}_x\right|^2-\left|\mathbf{E}_y\right|^2\right\rangle \\ S_2&=\left\langle 2\,\mathrm{Re}\left(\mathbf{E}^*_x\mathbf{E}_y\right)\right\rangle,\ S_3=\left\langle 2\,\mathrm{Im}\left(\mathbf{E}^*_x\mathbf{E}_y\right)\right\rangle \end{aligned} \tag{8}$$

where $\langle\cdot\rangle$ donates the mean value over time.

When ignoring the attenuation in a small segment Δz in SMF, S_0 remains unchanged. Then, normalizing the Stokes vectors, the vector $\mathbf{S}=\left(S_1 \quad S_2 \quad S_3\right)^{\mathrm{T}}$ can be presented in the Poincaré sphere. After that, distributed birefringence can be measured with (5).

3. Fine spatial resolution birefringence measurement with PC-Φ-OTDR

In this section, the linear birefringence measurement with fine spatial resolution is achieved using PC-Φ-OTDR.

The experimental setup is shown in Fig. 2. The linewidth of the 1550 nm laser is below 0.1 kHz. One output of the optical coupler 1 (OC1) goes through the attenuator and the polarization controller 1 (PC1), and it enters the 90° optical hybrid as the local oscillator [25]. The other output of the OC1 is modulated into chirped pulses by the I/Q modulator. Then, the chirped pulses are amplified by an erbium-doped fiber amplifier (EDFA). Fiber Bragg grating (FBG) is used to filter out the amplified

spontaneous emission (ASE) generated by the EDFA. The amplified chirped pulse passes through the PC2 to control its polarization state and is divided into two parts by OC2. The 10% part is used to detect the SOPs of the input lights by the polarization state analyzer (PSA).

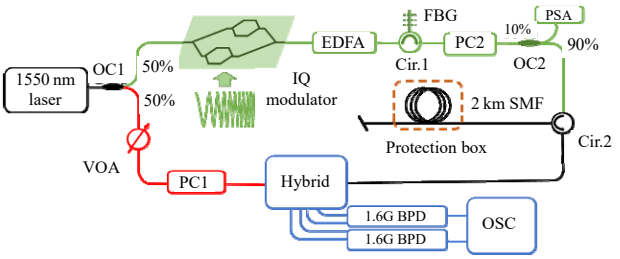

Fig. 2 Experimental setup of measuring the birefringence within 2 km SMF. OC: optical coupler; EDFA: erbium-doped fiber amplifier; FBG: fiber Bragg grating; Cir: circulator; PSA: polarization state analyzer; VOA: variable optical attenuator; PC: polarization controller; Hybrid: 90° optical hybrid; 1.6 G BPD: balanced photo-detector with 1.6 GHz bandwidth; OSC: oscilloscope.

Two 1.6 GHz balanced photo-detectors (BPDs) and oscilloscope (OSC) with 10 GHz sampling rate are used to collect the two orthogonal components of the beating signal. Using (6), the SOPs of the RBS lightwave are acquired. In order to eliminate the influences of the disturbance of external environment, the 2 km spun SMF is placed into a protection box.

In theory, PC-Φ-OTDR can achieve tens or even hundreds of kilometers of birefringence measurements. Here is an example of measuring two kilometers of SMF. As for the property of the probing pulse, the 50 MHz–1 250 MHz scan range is used (with 1.2 GHz bandwidth), corresponding to 8.6 cm spatial resolution. The pulse width is 15 μs, and the repetition period is 40 μs. In SMF, the PMD experienced by a pulse with 1.2 GHz bandwidth is ignorable [26].

The experimental results of birefringence distribution are shown in Fig. 3. In Fig. 3(a), the blue and orange curves show the birefringence along the whole fiber when the light is launched along the SOP 1 (P1) at different times. The sampling time interval between the two curves is about 3 minutes and the two curves' correlation coefficient is 0.93. The average birefringence along the whole fiber is 0.234 rad/m, which means the beat length is 26.9 m and the index difference is 5.8×10^{-8}. Figure 3(b) shows the measured birefringence with the launched lights along the SOP 1 (P1) and SOP 2 (P2), respectively. The time interval between Group 1 and Group 3 is around 6 minutes and the correlation coefficient is 0.89.

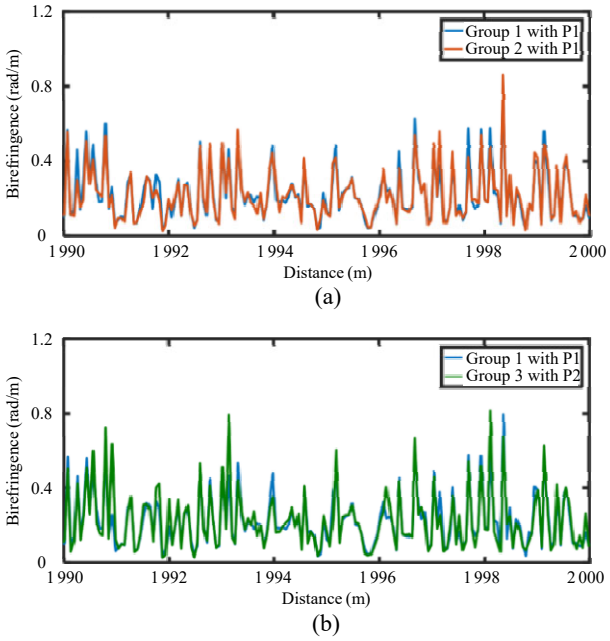

Fig. 3 Measurement results of birefringence: (a) two groups when the polarized light is launched along SOP 1 (P1) and (b) two groups when the polarized light is launched along P1 and SOP 2 (P2).

It is worth to emphasize that the P1 and P2 are randomly chosen by adjusting the PC. The locations of P1 and P2 on the Poincaré sphere are shown in Fig. 4, with an angular difference of 48°. The results show that this method has no dependence on the input SOP and has good repeatability. The measured distributed birefringence's mean equals to 0.234 rad/m in single-mode fiber, which corresponds to 26.9 m beat length. Similar results have been demonstrated in many reports. In 2000, a POTDR system was built using the Muller matrix method by Galtarossa *et al.* [14] to statistically characterize fiber random birefringence. The experimental result

showed that the average local birefringence of the fiber was 0.220 rad/m in the 17 km single-mode fiber under test, corresponding to a beat length of 28.5 meters. In 2015, Liu *et al.* [16] proposed and implemented the three-point quaternion method to measure birefringence distribution for single-mode fiber. The experimental result showed that the average birefringence was 0.236 rad/m in the 1 km single-mode fiber under test, and the corresponding average beat length was 26.6 meters. In 2019, Costa *et al.* [17] detailed a method of using chirped-pulse phase-sensitive optical time-domain reflectometry to directly measure linear birefringence of single-mode fibers. The experimental result showed that the average birefringence was 0.215 rad/m in the 4 km single-mode fiber under test, and the corresponding average beat length was 29.2 meters.

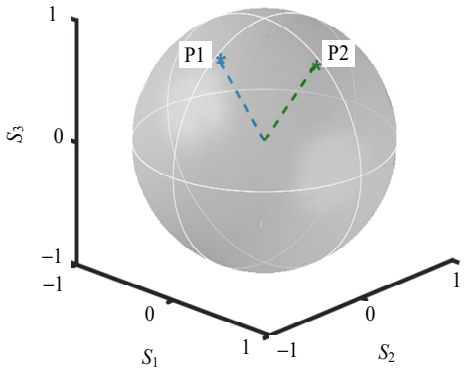

Fig. 4 Two launched lights' SOPs in the Poincaré sphere with an angular difference of 48°.

The above examples illustrate that for standard single-mode fiber, the fiber's beat length is almost 27 meters, which further proves the reliability of the measurement results in this paper. However, the above reports have only analyzed the measurement results of birefringence under the condition of single spatial resolution. After a series of simulations and experimental verifications, the results show that the measured birefringence is dependent on spatial resolution.

4. Birefringence measurement results with different spatial resolutions

In this section, simulations and experiments are elaborated to analyze the dependence of birefringence measurement on spatial resolution. In the PC-Φ-OTDR system, the relationship between the spatial resolution L and the bandwidth B can be expressed as $L = c/2nB$, where c is the speed of light in vacuum, and n is the index of the fiber, which equals to 1.5. In addition, 2 means the round trip of the RBS lightwave.

4.1 Simulation results

Reference [26] has summarized the three theoretical statistical models of linear birefringence: (1) the birefringence could be divided into two parts, with constant and deterministic one and white-noise random perturbed one [14]; (2) the modulus of the birefringence is assumed fixed, while its orientation varies according to Wiener process [27]; (3) both the modulus and the orientation of the birefringence are varied. The first two components of the local birefringence vector $\boldsymbol{\beta}(z) = (\beta_1 \quad \beta_2 \quad 0)^{\mathrm{T}}$ are assumed to be Gaussian random processes, respectively, with zero mean and same standard deviation [27]. Reference [26] also suggests that the third model is more reasonable. As a result, in our model, the modulus of $\boldsymbol{\beta}(z)$ is randomly distributed with the Rayleigh process.

In fact, the simulation model of PC-Φ-OTDR used here refers to the simulation model of traditional Φ-OTDR, but there are two main differences. On the one hand, the type of incident light is changed from single pulse to chirped pulse. On the other hand, the scattering element is changed from one-dimensional to two-dimensional, assuming that each scattering element has two polarization principal axes. A more detailed explanation of the simulation model will be presented in the subsequent report. In the simulation model, the fiber is 200 m, and the mean value of birefringence is 0.230 rad/m, which means the beat length is 27.3 meters. Assume that the fiber has a sequence of independent elements every 1 mm.

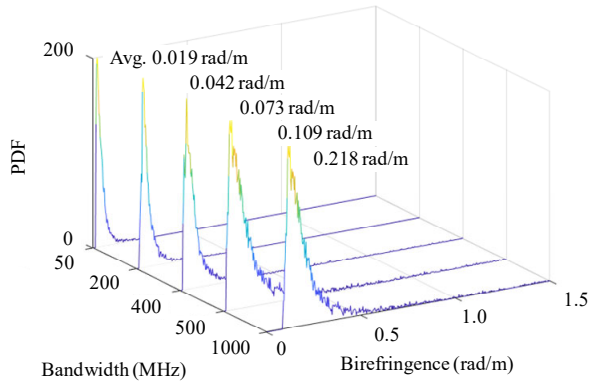

Fig. 5 Probability density function of the demodulated birefringence with different bandwidths.

Figure 5 shows the probability density function (PDF) of the demodulated birefringence with five different bandwidths of the probing chirped-pulse, 50 MHz, 200 MHz, 400 MHz, 500 MHz, and 1 000 MHz, and the corresponding spatial resolutions are 2 m, 0.5 m, 0.25 m, 0.2 m, and 0.1 m, respectively. Their PDFs all show Rayleigh distribution [28], with the mean values of 0.218, 0.109, 0.073, 0.042, and 0.019, respectively. This results show that the demodulated birefringence is linearly related to the incident bandwidth.

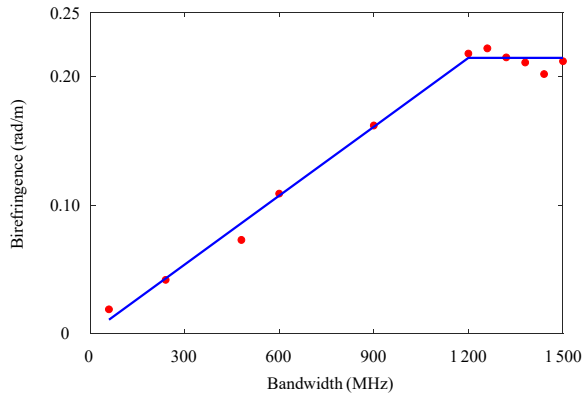

Fig. 6 Demodulated birefringence with different bandwidths.

In order to further investigate the relationship between the bandwidth of the incident light and the demodulated birefringence, a series of different bandwidths are simulated. Figure 6 shows the demodulated birefringence with an increase in the incident light bandwidth, where the blue curve is a fitted line of the simulation results. The results show that within a relatively small bandwidth, the demodulated birefringence through backscattered SOP increases with an increase in the bandwidth. After exceeding a certain bandwidth, the demodulated birefringence nearly keeps constant as the change of bandwidth.

4.2 Experimental results

The statistical distribution of birefringence in different bandwidths is obtained through experiments as shown in Fig. 7. In this figure, it contains statistical distributions of birefringence four different chirped pulses, with bandwidths of 100 MHz, 500 MHz, 800 MHz, and 1 200 MHz, respectively. These pulses have the same 500 ns pulse width and 15 μs repeat period. Different bandwidths would obtain different birefringence, but the birefringence distributions all conform to the Rayleigh distribution, and the change rule of the demodulated birefringence is consistent with the simulation results.

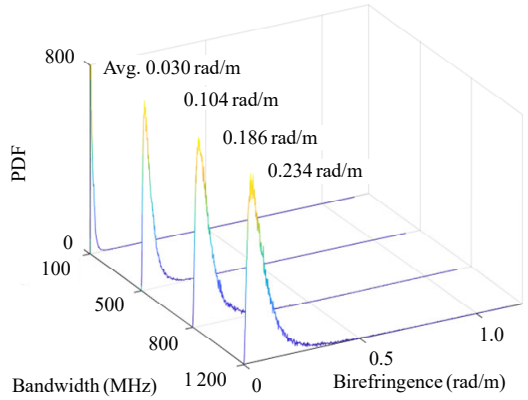

Fig. 7 PDFs of the demodulated birefringence with different bandwidths.

Figure 8 depicts that the mean value of demodulated birefringence is related to the bandwidth, where the blue dots and the red diamonds represent the experiments and simulations, respectively. The blue curve is the fitted line from simulation results. The experimental results show that by constantly increasing the incident light bandwidth, demodulated birefringence is higher, and the birefringence keeps constant after passing a certain bandwidth like the simulation results. Unfortunately, due to the hardware limitations, the

sweep frequency bandwidth of 1.2 GHz is the largest we can achieve. Since the experimental results agree with the simulation results, it can be concluded that when the bandwidth is smaller than a certain value, the measured birefringence is linearly related to the bandwidth. When the bandwidth exceeds a certain value, the measured birefringence remains unchanged.

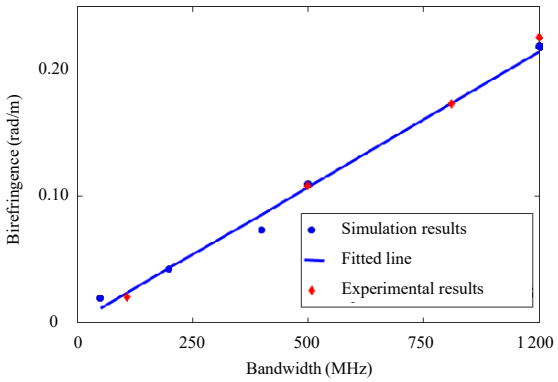

Fig. 8 Demodulated birefringence of simulation and experiments.

4.3 Discussion

As the results shown in Section 4.2, the measured birefringence measured with different spatial resolutions is also different. Perhaps the most intuitive thought is that the smaller spatial resolution is, the smaller measured birefringence is, but the results here are opposite (higher values of birefringence are got from smaller spatial resolution). The reason of this phenomenon is that the optical fiber under test is a spun fiber, which is rotated during the drawing so as to change the fiber birefringence axes in period. It is one of the most effective ways to reduce PMD [29]. Palmieri [30] had carefully analyzed the polarization properties of spun fiber, and he pointed out that the spun fiber introduces larger birefringence locally during the manufacturing process to reduce the beat length and mitigate the overall polarization effect of the optical fiber. In addition, for spun fibers, the rotation process does not introduce circular birefringence, so it does not have any additional influence on the above-mentioned experimental process and results.

5. Conclusions

Birefringence is a stochastic parameter in the fibers and it is sensitive to internal and external perturbations, such as bending, stressing, and twisting. As a result, measuring the distribution of birefringence with high fidelity is difficult. However, the currently known systems for measuring birefringence require incident light not only with several specific SOPs to complete a measurement but also with insufficient measurement accuracy.

In this paper, a novel measuring method for the distribution of birefringence is proposed. PC-ΦOTDR has been implemented with 8.6 cm spatial resolution to measure the 2 km spun single-mode fiber, of which the average birefringence equals to 0.234 rad/m. This system only needs a chirped pulse to retrieve the birefringence without adjusting the SOP. Besides, it is the first time that the relationship between spatial resolution and measured birefringence has been explored and carefully described both from simulations and experiments. This work provides an effective tool for characterizing the polarization properties of optical-fiber link.

References

[1] A. Galtarossa and L. Palmieri, “Distributed polarization sensing,” in *25th International Conference on Optical Fiber Sensors*, Jeju, Korea, 2017, pp. 1032318.

[2] S. Rashleigh, “Origins and control of polarization effects in single-mode fibers,” *Journal of Lightwave Technology*, 1983, 1(2): 312–331.

[3] A. Wegmuller, M. Legre, and N. Gisin, “Distributed beatlength measurement in single-mode fibers with optical frequency-domain reflectometry,” *Journal of Lightwave Technology*, 2002, 20(5): 828–835.

[4] A. M. Kurbatov and R. A. Kurbatov, “Polarization

and modal filters based on W-fibers panda for fiber-optic gyroscopes and high-power fiber lasers," *Optical Engineering*, 2013, 52(3): 035006.

[5] R. Wang, S. Xu, W. Li, and X. Wang, "Optical fiber current sensor research: review and outlook," *Optical and Quantum Electronics*, 2016, 48(9): 442.

[6] B. E. Olsson, M. Karlsson, and P. A. Andrekson, "Polarization mode dispersion measurement using a Sagnac interferometer and a comparison with the fixed analyzer method," *IEEE Photonics Technology Letters*, 1998, 10(7): 997–999.

[7] X. Fang and R. O. Claus, "Polarization-independent all-fiber wavelength-division multiplexer based on a Sagnac interferometer," *Optics Letters,* 1995, 20(20): 2146–2148.

[8] C. S. Kim, Y. G. Han, R. M. Sova, U. C. Paek, Y. Chung, and J. U. Kang, "Optical fiber modal birefringence measurement based on Lyot-Sagnac interferometer," *IEEE Photonics Technology Letters*, 2003, 15(2): 269–271.

[9] Z. Ren, Y. Wang, and P. A. Robert, "Faraday rotation and its temperature dependence measurements in low-birefringence fibers," *Journal of Lightwave Technology*, 1989, 7(8): 1275–1278.

[10] M. Segura, N. Vukovic, N. White, W. H. Loh, F. Poletti, *et al.*, "Low birefringence measurement and temperature dependence in meter-long optical fibers," *Journal of Lightwave Technology*, 2015, 33(12): 2697–2702.

[11] L. Thévenaz, M. Facchini, A. Fellay, M. Niklès, and P. Robert, "Evaluation of local birefringence along fibres using Brillouin analysis," in *Conference Digest OFMC'97*, Teddington, UK, 1997, pp: 82–85.

[12] Y. Lu, X. Bao, L. Chen, S. Xie, and M. Pang, "Distributed birefringence measurement with beat period detection of homodyne Brillouin optical time-domain reflectometry," *Optics Letters*, 2012, 37(19): 3936–3938.

[13] A. J. Rogers, "Polarization-optical time domain reflectometry: a technique for the measurement of field distributions," *Applied Optics*, 1981, 20(6): 1060–1074.

[14] A. Galtarossa, L. Palmieri, M. Schiano, and T. Tambosso, "Statistical characterization of fiber random birefringence," *Optics Letters*, 2000, 25(18): 1322–1324.

[15] M. A. Soto, X. Lu, H. F. Martins, M. Gonzalez-Herraez, and L. Thévenaz, "Distributed phase birefringence measurements based on polarization correlation in phase-sensitive optical time-domain reflectometers," *Optics Express*, 2015, 23(19): 24923–24936.

[16] L. Liu, C. Wu, C. Shang, Z. Li, and J. Wang, "Quaternion approach to the measurement of the local birefringence distribution in optical fibers," *IEEE Photonics Journal*, 2015, 7(4): 1–14.

[17] L. Costal, R. Magalhaes, L. Palmieri, H. Martins, S. Martin-Lopez, M. R. Fernández-Ruiz, *et al.*, "Fast and direct measurement of the linear birefringence profile in standard single-mode optical fibers," *Optics Letters*, 2020, 45(3): 623–626.

[18] J. Xiong, J. Jiang, Y. Wu, Y. Chen, L. Xie, Y. Fu, *et al.*, "Chirped-pulse coherent-OTDR with predistortion," *Journal of Optics*, 2018, 20(3): 034001.

[19] F. Corsi, A. Galtarossa, and L. Palmieri, "Analytical treatment of polarization-mode dispersion in single-mode fibers by means of the backscattered signal," *Journal of the Optical Society of America A*, 1999, 16(3): 574–583.

[20] Z. Wang, Y. Fu, X. Qian, L. Zhang, and Y. Rao, "Proposal for distributed measurement of Müller matrix in optical fibers," in *2016 15th International Conference on Optical Communications and Networks (ICOCN)*, China, Sept. 24–27, 2016, pp: 1–3.

[21] Z. Yu, X. Yi, Q. Yang, M. Luo, J. Zhang, L. Chen, *et al.*, "Polarization demultiplexing in stokes space for coherent optical PDM-OFDM," *Optics Express*, 2013, 21(3): 3885–3890.

[22] M. Ren, P. Lu, L. Chen, and X. Bao, "Theoretical and experimental analysis of Φ-OTDR based on polarization diversity detection," *IEEE Photonics Technology Letters*, 2015, 28(6): 697–700.

[23] J. Jiang, Z. Wang, Z. Wang, Y. Wu, S. Lin, J. Xiong, *et al.*, "Coherent Kramers-Kronig receiver for Φ-OTDR," *Journal of Lightwave Technology*, 2019, 37(18): 4799–4807.

[24] A. Kumar and A. K. Ghatak, *Polarization of light with applications in optical fibers*. Washington, USA: SPIE Press, 2011: 98–118.

[25] Z. Wang, L. Zhang, S. Wang, N. Xue, F. Peng, M. Fan, *et al.*, "Coherent *Φ*-OTDR based on I/Q demodulation and homodyne detection," *Optics Express*, 2016, 24(2): 853–858.

[26] A. Galtarossa and L. Palmieri, "Reflectometric measurements of PMD properties in long single-mode fibers," *Optical Fiber Technology*, 2003, 9(3): 119–142.

[27] G. J. Foschini and C. D. Poole, "Statistical theory of polarization dispersion in single mode fibers," *Journal of Lightwave Technology*, 1991, 9(11): 1439–1456.

[28] P. K. A. Wai and C. R. Menyak, "Polarization mode dispersion, decorrelation, and diffusion in optical fibers with randomly varying birefringence," *Journal of Lightwave Technology*, 1996, 14(2): 148–157.

[29] M. J. Li and D. A. Nolan, "Fiber spin-profile designs for producing fibers with low polarization mode dispersion," *Optics Letters*, 1998, 23(21): 1659–1661.

[30] L. Palmieri, "Polarization properties of spun single-mode fibers," *Journal of Lightwave Technology*, 2006, 24(11): 4075–4088.